*Progress In Electromagnetics Research Letters, Vol. 61, 1–6, 2016*

# Dual-Band Printed Inverted-F Antenna with a Nested Structure

**Takuichi Hirano*** **and Junichi Takada**

**Abstract**—A dual-band printed inverted-F antenna with a nested structure is proposed. In this antenna, matching can be controlled for both frequency bands by changing element lengths. The measured and calculated frequency characteristics of the antenna's reflection coefficient match very well, if the measurement cable connector is considered in the simulation. The measured −10 dB relative bandwidths of the reflection coefficient are 4.7% at 2.45 GHz (2.5 GHz to 2.62 GHz), and 9% at 5.5 GHz (5.28 GHz to 5.78 GHz). The calculated radiation efficiencies are 92% and 88%, at 2.45 GHz and 5.5 GHz, respectively, with calculated peak realized gains of 1.07 dBi and 3.36 dBi, respectively.

## 1. INTRODUCTION

Inverted-F antennas [1, 2] are widely used because of their compact, low profile features [3, 4]. They are also used in wireless LAN (local area network) applications, because they can be easily integrated with dielectric substrates, or printed circuit boards. There are two widely used unlicensed bands (2 GHz and 5 GHz) for wireless LANs, and there is a strong demand for compact antennas covering both these frequency bands. A dual-band printed inverted-F type antenna [5] has been proposed for this purpose. However, with the structure presented in [5], the design parameters for each one of the two bands are not explicit.

In this study, a dual-band printed inverted-F antenna with a nested structure is proposed (see Fig. 1). In this antenna, matching can be controlled for both frequency bands by changing element lengths.

## 2. DUAL-BAND PRINTED INVERTED-F ANTENNA

Figure 1 shows the configuration of a dual-band printed inverted-F antenna. An FR-4 (Panasonic R-1705) is used as the substrate. A 50 Ω microstrip line with a 3-milimiter-wide signal line is used for feeding the antenna. Two F-shaped patterns are nested in the upper metal layer. The longer element is used for the lower frequency band, and the shorter one for the higher band. Two via holes with a diameter of 1.27 mm connect the upper and lower metal layers. A Sub-Miniature version A (SMA) connector (shown in Fig. 2) is installed on the edge of the substrate, and used for measurement. The inner and outer conductors are connected to the upper and lower conductor layers of the FR-4 substrate, respectively. Both the SMA connector and the FR-4 substrate material properties are modeled (for simulation purposes) as in [6].

*Received 12 April 2016, Accepted 27 May 2016, Scheduled 6 June 2016*
* Corresponding author: Takuichi Hirano (hira@ide.titech.ac.jp).
The authors are with the Department of Transdisciplinary Science and Engineering, School of Environment and Society, Tokyo Institute of Technology, S6-4, 2-12-1, O-okayama, Meguro-ku, Tokyo 152-8552, Japan.

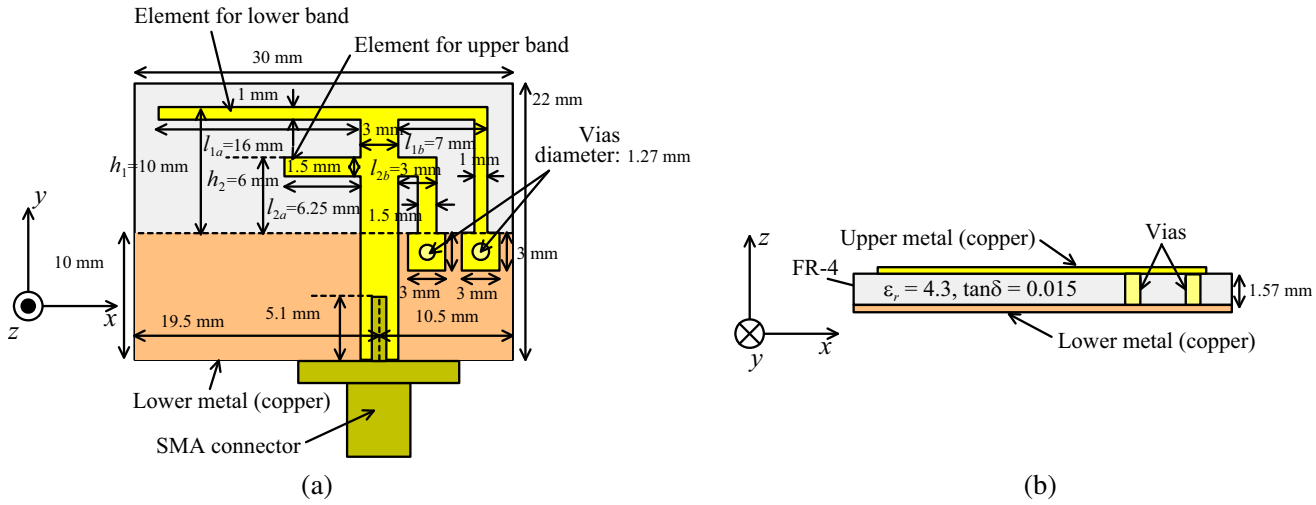


**Figure 1.** Configuration of the dual-band printed inverted-F antenna. (a) Top view. (b) Cross sectional view.

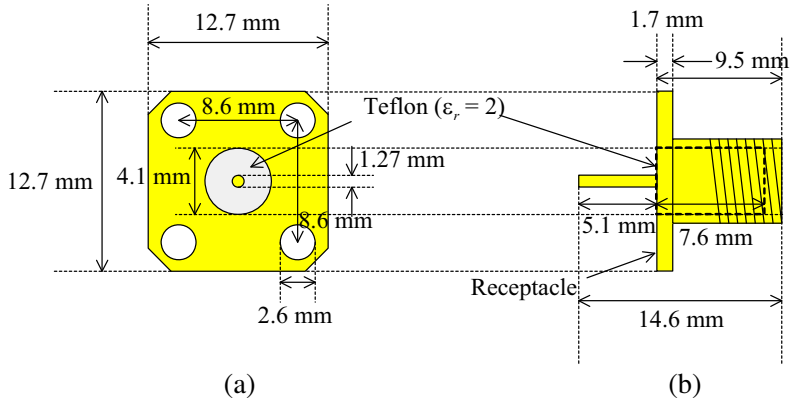


**Figure 2.** SMA connector dimensions. (a) Top view. (b) Side view.

## 3. PARAMETRIC STUDY

The dual-band printed inverted-F antenna was designed by choosing parameters $l_{1a}$, $l_{1b}$, $h_1$, $l_{2a}$, $l_{2b}$, $h_2$, and line widths (see Fig. 1). As an example, a dual-band printed inverted-F antenna resonating at 2.45 GHz and 5.5 GHz was designed. A finite element simulator (ANSYS HFSS, version 11) was used in this study. To obtain design guidelines, a parametric study was conducted by changing $l_{1a}$, $l_{1b}$, $h_1$, $l_{2a}$, $l_{2b}$, and $h_2$ from a chosen set of base parameters. The frequency characteristics of the reflection coefficient for three different values of $l_{1a}$, $l_{1b}$, $h_1$, $l_{2a}$, $l_{2b}$, and $h_2$ are shown in Fig. 3, Fig. 4, Fig. 5, Fig. 6, Fig. 7, and Fig. 8, respectively.

As shown, the frequency characteristic is insensitive to $l_{1b}$ and $l_{2b}$. The lower and higher resonant frequencies can be controlled by changing $l_{1a}$ and $l_{2a}$, respectively. $h_1$ affects both resonant frequencies, but these frequency values can be compensated by other parameters ($l_{1a}$ and $l_{2a}$). Through $h_1$ and $h_2$, antenna matching in the lower and higher frequency bands, respectively, can be controlled.

## 4. RESULTS

A photograph of the manufactured antenna is shown in Fig. 9, and its HFSS analysis models are shown in Fig. 10. Fig. 11 shows the calculated and obtained frequency characteristics of the reflection coefficient. A frequency shift between the measured (exp.) and calculated (cal. (w/o cable)) results can

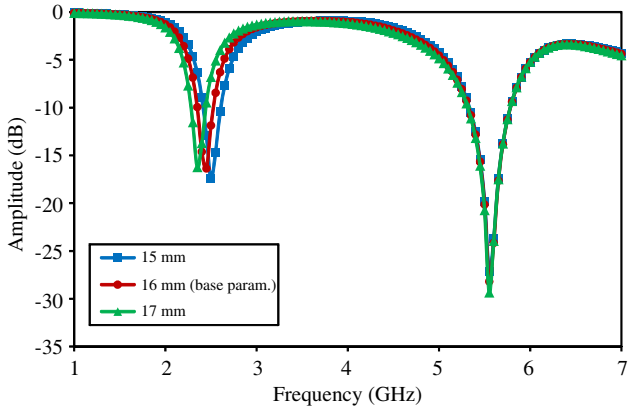


**Figure 3.** Frequency characteristics of the reflection coefficient for three different values of $l_{1a}$ (calculated).

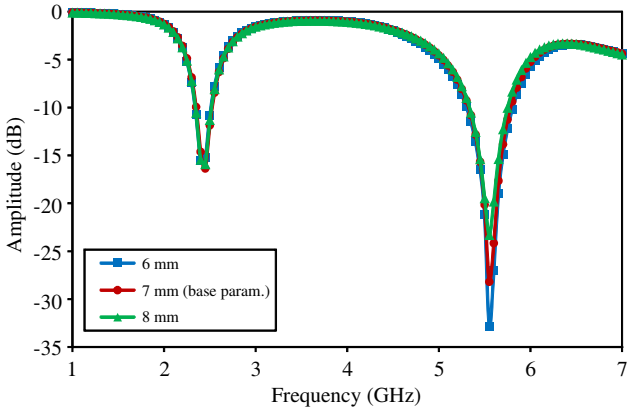


**Figure 4.** Frequency characteristics of the reflection coefficient for three different values of $l_{1b}$ (calculated).

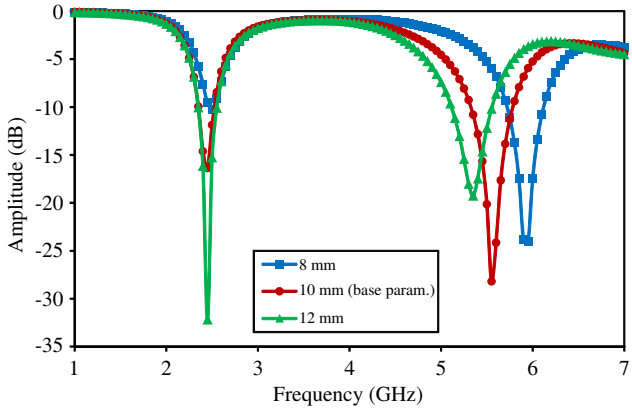


**Figure 5.** Frequency characteristics of the reflection coefficient for three different values of $h_1$ (calculated).

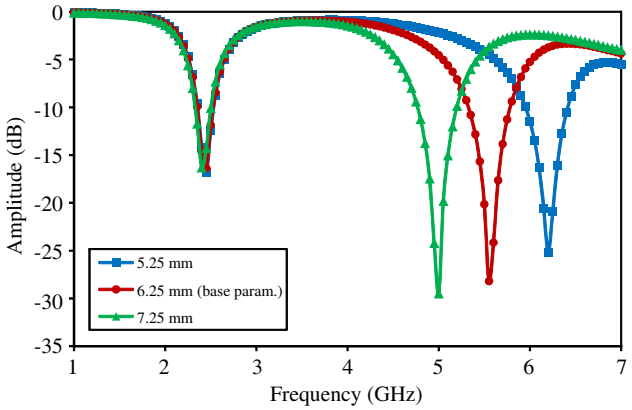


**Figure 6.** Frequency characteristics of the reflection coefficient for three different values of $l_{2a}$ (calculated).

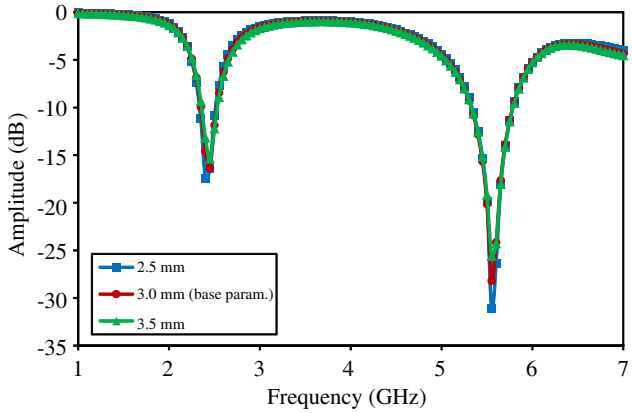


**Figure 7.** Frequency characteristics of the reflection coefficient for three different values of of $l_{2b}$ (calculated).

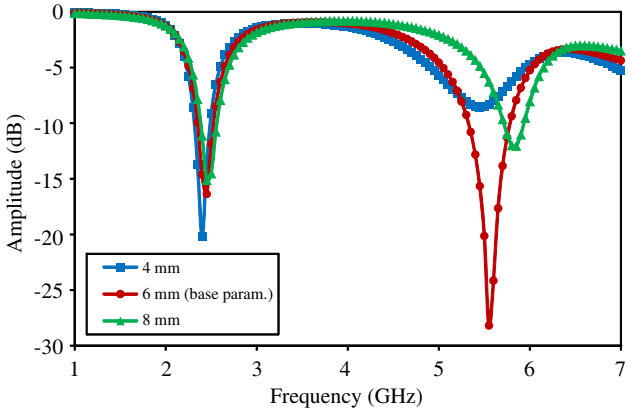


**Figure 8.** Frequency characteristics of the reflection coefficient for three different values of of $h_2$ (calculated).

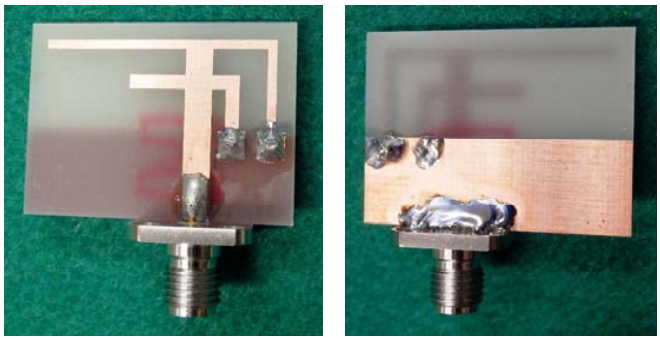

(a) (b)

**Figure 9.** Photograph of the developed antenna. (a) Top view. (b) Bottom view.

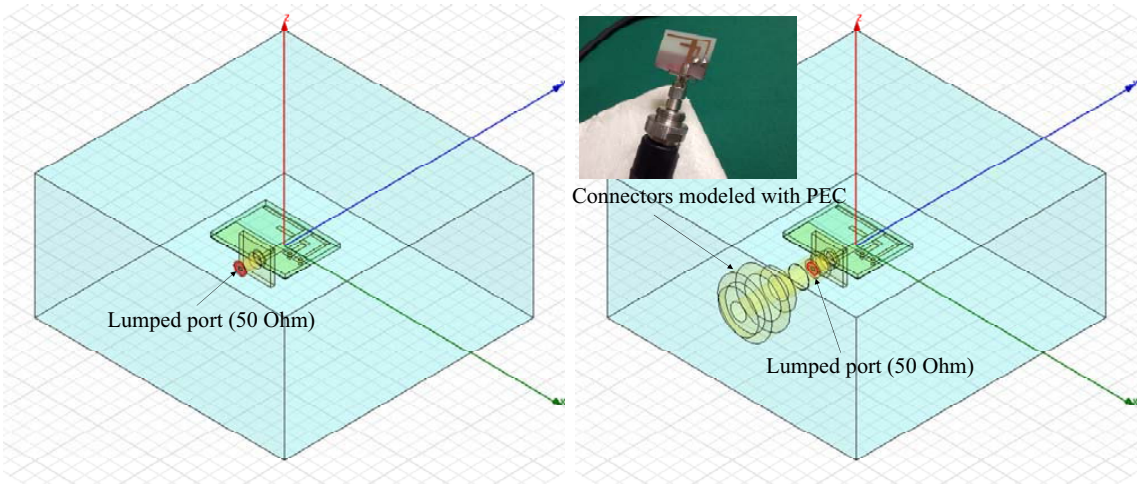


(a) (b)

**Figure 10.** HFSS analysis models. Absorbing conditions are imposed at all external boundaries (radiation boundary). (a) w/o cable. (b) w/ cable.

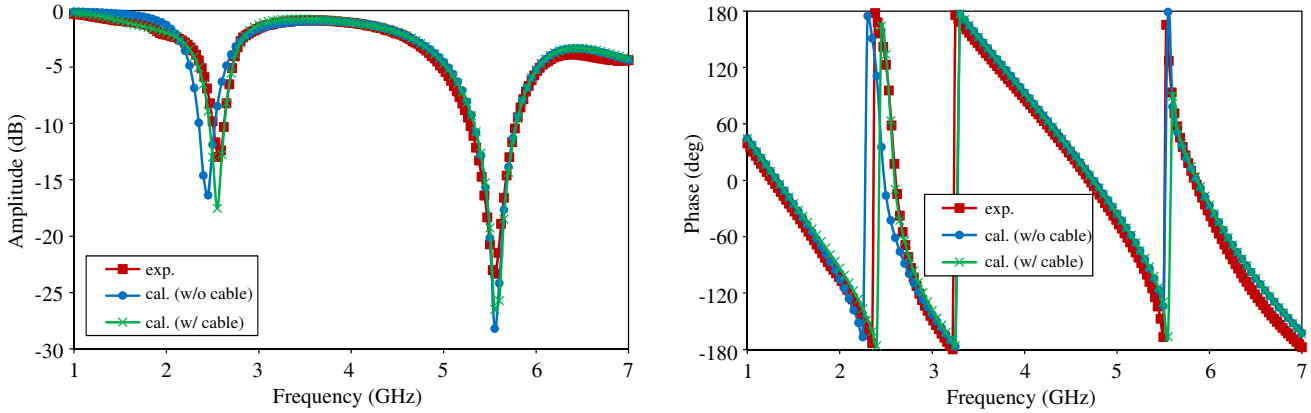


(a) (b)

**Figure 11.** Calculated and obtained frequency characteristics of the reflection coefficient. (a) Amplitude. (b) Phase.

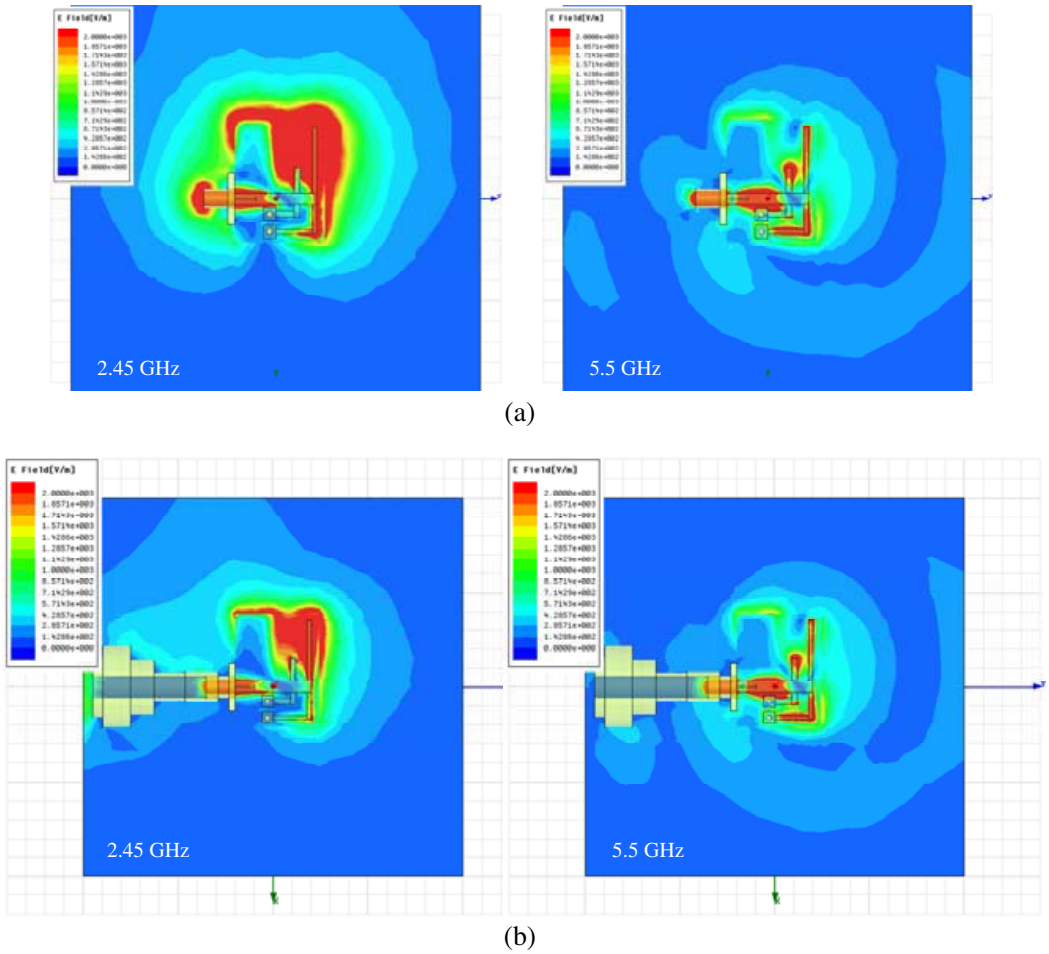


**Figure 12.** Calculated electric field distribution in the $x$-$y$ plane (a snapshot of time). (a) w/o cable. (b) w/ cable.

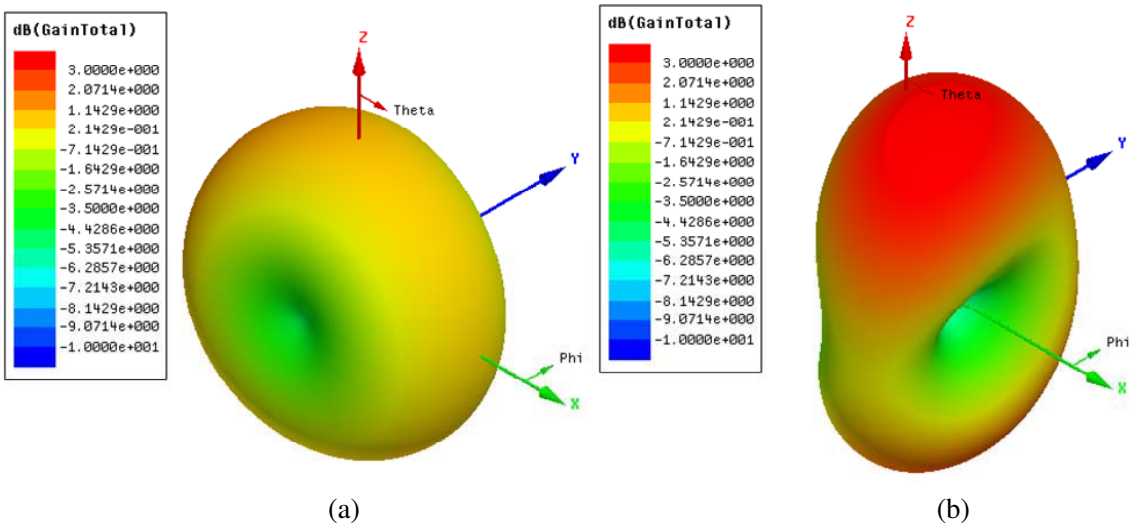


**Figure 13.** Calculated 3-D gain patterns. (a) 2.45 GHz. (b) 5.5 GHz.

be observed at the lower frequency band (2.45 GHz). This shift is due to the cable connectors used for measurement in the experimental setup, shown in Fig. 10(b); when the model in Fig. 10(b) was used, the calculated results (cal. (w/ cable)) matched very well with the measured values. The importance of cable connector modeling can be explained by considering electromagnetic field scattering. Fig. 12 shows calculated electric field distribution in the $x$-$y$ plane. The difference of electric field distribution between two models (w/o cable and w/ cable) is significant at 2.45 GHz while it is not significant at 5.5 GHz. Therefore the modeling of the cable connector, not only the SMA connector [6], is important at 2.45 GHz due to strong perturbation of the field. The measured $-10$ dB relative bandwidths of the reflection coefficient were 4.7% at 2.45 GHz (2.5 GHz to 2.62 GHz), and 9% at 5.5 GHz (5.28 GHz to 5.78 GHz). Although the working band 2.5 GHz–2.62 GHz is out of IEEE 802.11b/g/n 2.4 GHz frequency band, the frequency band can be adjusted by changing $l_{1a}$ for variety of implementations.

Figure 13 shows the calculated 3-D gain patterns for the model in Fig. 10(a). The calculated radiation efficiencies were 92% and 88%, at 2.45 GHz and 5.5 GHz, respectively, with calculated peak realized gains of 1.07 dBi and 3.36 dBi, respectively.

## 5. CONCLUSION

A dual-band printed inverted-F antenna with a nested structure was proposed, in which matching can be controlled for both bands by changing element lengths. The measured and calculated frequency characteristics of the reflection coefficient match very well, if the measurement cable connector is considered in the simulation. Measured relative bandwidths (at $-10$ dB) of 4.7% and 9% were obtained for the reflection coefficient, at 2.45 GHz and 5.5 GHz, respectively. The calculated radiation efficiencies at these frequencies were 92% and 88%, with calculated peak realized gains of 1.07 dBi and 3.36 dBi, respectively.

## ACKNOWLEDGMENT

This work was supported in part by MEXT/JSPS KAKENHI (Grant number 26820139) and in part by the Japan Agency for Medical Research and Development (AMED). Measurements were performed in Ando and Hirokawa Lab. of Tokyo Institute of Technology.

## REFERENCES

1. King, R. W. P., C. W. Harrison, Jr., and D. H. Denton, Jr., "Transmission-line missile antennas," *Sandia Corp. Technical Memo.*, Vol. 14, 436–458, November 1958.
2. King, R. W. P., C. W. Harrison, Jr., and D. H. Denton, Jr., "Transmission-line missile antennas," *IRE Transactions on Antennas and Propagation*, Vol. 8, No. 1, 88–90, January 1960.
3. Waterhouse, R., *Printed Antennas for Wireless Communications*, John Wiley & Sons, Pharad, Maryland, 2008.
4. Soras, C., M. Karaboikis, G. Tsachtsiris, and V. Makios, "Analysis and design of an inverted-F antenna printed on a PCMCIA card for the 2.4 GHz ISM band," *IEEE Antennas and Propagation Magazine*, Vol. 44, No. 1, 37–44, February 2002.
5. Rennings, A., M. Rauf, P. Waldow, and I. Wolff, "A compact single/dual-band printed inverted-F type antenna structure," *ACES, Advanced Computational Techniques for Antenna Design*, April 2004.
6. Hirano, T., J. Hirokawa, and M. Ando, "Influence of the SMA connector and its modeling on electromagnetic simulation," *Microwave and Optical Technology Letters (MOP)*, Vol. 57, No. 9, 2168–2171, September 2015.